Electronic Supplementary Material (ESI) for Physical Chemistry Chemical Physics.

Supplementary information

Thickness dependent homogeneous crystallization of ultrathin amorphous solid water films

Kuniaki Harada, Toshiki Sugimoto, Fumiaki Kato, Kazuya Watanabe, and Yoshiyasu Matsumoto

1. Estimation of fraction crystallized in the film

2. Isothermal crystallization at surface and in bulk

3. Comparison of crystallization time with those obtained in previous reports

4. Vibrational signature of H_2O superstructure on Pt(111)

5. Activation energy of crystallization and Avrami index as a function of film thickness

1. Estimation of fraction crystallized in the film

To obtain the temperature dependence of bulk crystallinity quantitatively, we evaluated the fraction crystallized in bulk (x_{bulk}) by deconvoluting IRAS spectra $S(\omega)$ into two spectral components: $S_{ASW}(\omega)$ of ASW and $S_{CI}(\omega)$ of CI component.[1-3] Figure S1 shows the IRAS spectra of 18 ML ASW film at 148, 151, 152, and 156 K (from top to bottom) simultaneously taken during a TPD measurement. Dashed lines in Figure S1 represent the fitting results of the IRAS spectra by a linear combination of $S_{ASW}(\omega)$ and $S_{CI}(\omega)$ as

$$S(\omega,T) = A(T)\{x_{bulk}(T)\cdot S_{CI}(\omega) + (1 - x_{bulk}(T))\cdot S_{ASW}(\omega)\}, \qquad (S1)$$

where A is a proportional constant corresponding to the film thickness.

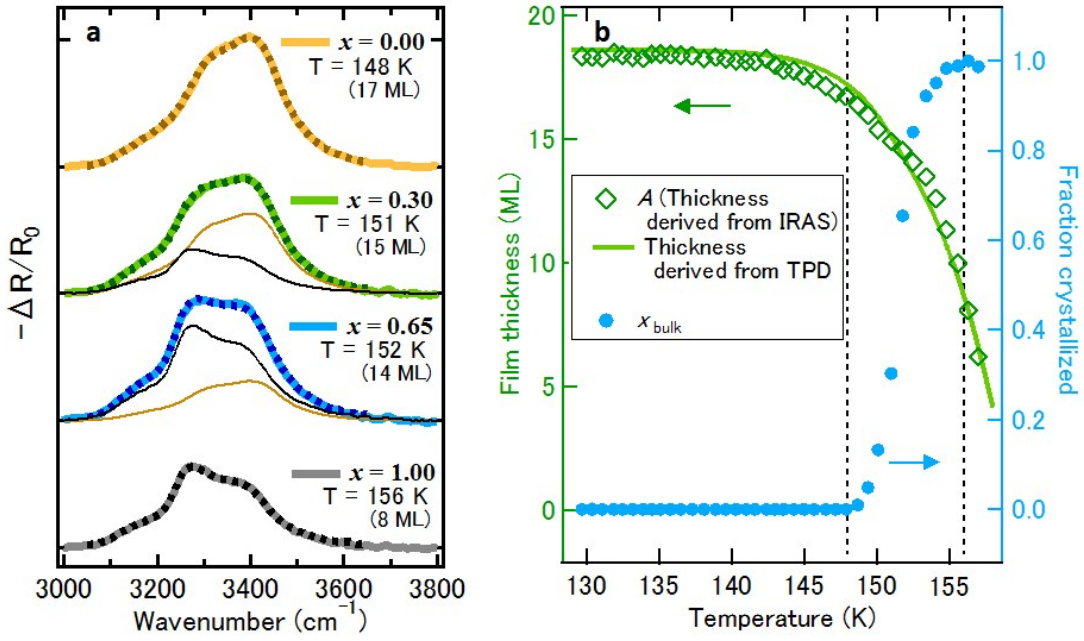

Figure S1. (a) Deconvolution of IRAS spectra into ASW (top) and CI (bottom) components. These spectra were taken during a TPD measurement at a heating rate of 0.1 K/s for the ASW film with initial thickness of 18 ML grown at 110 K. Dashed lines are the fitting results using a linear combination of the two spectral components. (b) Temperature dependence of A and x_{bulk} derived from the curve fitting. The region between two black dashed vertical lines represents the temperature range where crystallization proceeds. Thickness derived from the TPD trace (Figure 1a) is also shown for comparison.

Because the OH stretching band profile of H_2O films depends on the film thickness due to the flexible thickness-dependent structural change in the ultrathin hydrogen-bond network discussed in the main text (Figure 4), we need to take account of the thickness dependence of $S_{ASW}(\omega)$ and $S_{CI}(\omega)$. Figure S2 shows the peak normalized IRAS spectra of ASW and CI films. In the H_2O ASW spectra (Figure S2a), the relative intensity at 3300 cm^{-1} increases with increasing thickness while those at 3050 and 3550 cm^{-1} decrease. In contrast to the decoupled OH stretching vibration of HDO molecules in D_2O ice, the spectral shape of OH stretching of neat H_2O ice is significantly affected by the intramolecular vibrational coupling in H_2O and intermolecular coupling among OH moieties;[4-6] this makes the hydrogen-bonded OH-stretch bands of neat H_2O ice rather complicated. In the case of H_2O CI, the relative intensity of the shoulder peak at 3370 cm^{-1} decreases with increasing thickness from 5 to 18 ML (Figure S2b), as observed in the previous IRAS study of OD stretching band of D_2O CI.[7]

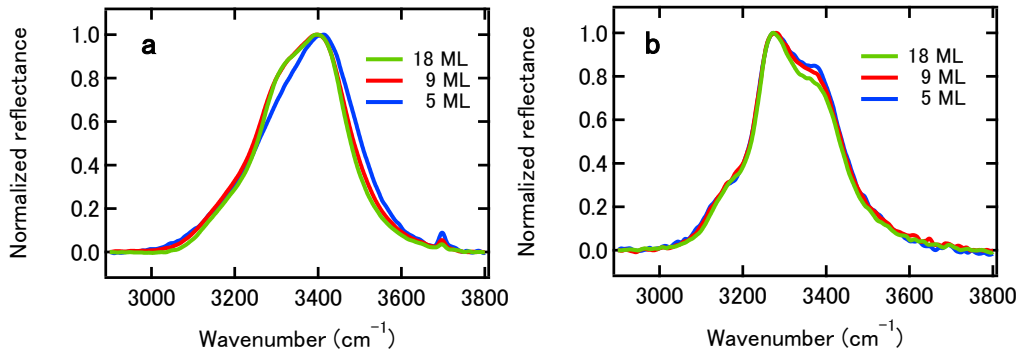

Figure S2. Thickness dependence of IRAS spectra of (a) H_2O ASW and (b) H_2O CI films. Each spectrum is normalized at its peak.

To take the thickness dependence into account, we used a linear combination of the two thickness-normalized spectra as follows,

$$S(\omega,T) = A(T)\left[x_{bulk}(T)\cdot\frac{S_{CI}(\omega;\theta_{CI})}{\theta_{CI}} + \left(1-x_{bulk}(T)\right)\cdot\frac{S_{ASW}(\omega;\theta_{ASW})}{\theta_{ASW}}\right], \qquad (S2)$$

where $S_{CI}(\omega;\theta_{CI})$ and $S_{ASW}(\omega;\theta_{ASW})$ are the spectra of ASW films grown at 110 K and CI films annealed at 155 K measured separately at the thickness of θ_{ASW} and θ_{CI}, respectively. Figure S1b shows the temperature dependence of A and x_{bulk} of the H_2O ASW film with an initial thickness of 18 ML. To confirm the accuracy in estimating the film thickness with Eq. S2, we also plot in Figure S1b the temperature dependence of the film thickness derived from the TPD trace of 18 ML ASW film (Figure 1a): the temperature dependences obtained with these different methods agree well with each other.

2. Isothermal crystallization at surface and in bulk

Figure S3a shows ITD traces for 31 ML H_2O ASW films at 148 K. The time evolutions of x_{surf} and x_{bulk} derived from the deconvolution of ITD traces and *in-situ* IRAS are shown in Figure S3b. Both x_{surf} and x_{bulk} changed simultaneously in the isothermal process as in the heating process (Figure 2), indicating that the entire films are crystallized homogeneously.

The effect of deposition rate on the crystallization mechanism was also investigated. Figure S4 shows the time evolutions of x_{surf} and x_{bulk} during the isothermal crystallization of the ASW ultrathin films deposited with a rate of 0.3 ML/s. Similar time evolutions of x_{surf} and x_{bulk} indicate homogeneous nucleation and crystallization of this film as those deposited at 0.02ML/s (Figure 2 and S3). Therefore, deposition rate does not affect the crystallization kinetics and mechanism of ASW ultrathin films in our experimental condition.

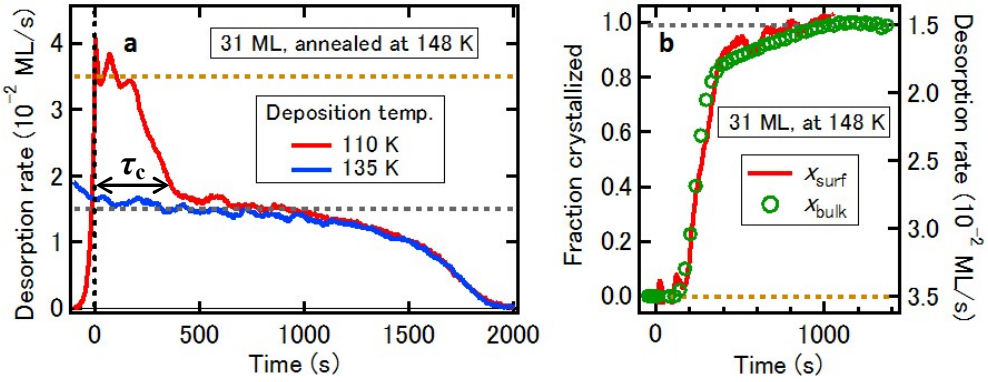

Figure S3. (a) ITD profiles of 31 ML ASW (red) and crystalline-ice (blue) films annealed at 148 K, and (b) time evolution of x_{surf} and x_{bulk}. Definition of the crystallization time τ_c is given in (a).

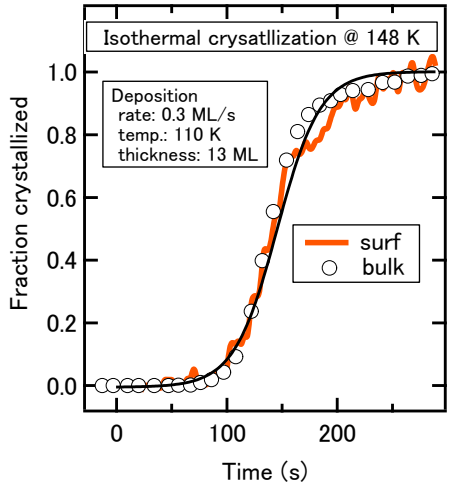

Figure S4. Time evolution of fraction crystallized at surface (green line) and in bulk (red open circles) probed in the isothermal crystallization process at 148 K for 13 ML ASW films deposited on Pt(111) at 110 K with a deposition rate of 0.3 ML/s.

3. Comparison of crystallization time and temperature with those obtained in previous reports

We monitored isothermal crystallization of ASW ultrathin films on Pt(111) grown at 110 K using IRAS. Figure S5a shows the thickness dependence of crystallization time τ_c at 145 K of the current study (red cross) together with that reported previously (black cross).[8,9] Here τ_c is defined as the time required for complete crystallization as shown in Figure S3(a). The previous result was obtained by ITD at 145 K for ASW films on Pt(111) grown at 100 K and is quantitatively consistent with our results. Löfgren and Ahlström et al. proposed only on the basis of this ITD measurement that the crystallization is initiated at the ASW/Pt(111) interface and proceeds heterogeneously.[8,9] However, our results definitely show that this kind of thickness dependent crystallization is initiated by *homogeneous nucleation* and proceeds homogeneously (Figures 2, S3b and S4).

Figure S5b shows thickness dependent changes of isothermal crystallization kinetics of ASW ultrathin films on Ru(0001), Au(111) and graphite in comparison with those on Pt(1111).[8-11] τ_c of ASW films on these substrates shows similar thickness dependence: it markedly increases as the thickness of the ultrathin film increases from ~5 ML to ~20 ML, while it levels off and converges to the constant value τ_{c-max} above around ~20 ML. While it is expected from the similar thickness profiles that the crystallization processes of ASW ultrathin films grown on other substrates may also be initiated by homogeneous nucleation as those on Pt(111), we cannot explicitly conclude the crystallization mechanism on other substrates without conducting simultaneous measurements of thermal desorption and IRAS. Because the relationship between hydrophobicity of substrates and the crystallization mechanism and kinetics of ASW nanofilms is a controversial issue,[12-17] further detailed investigation is necessary for definitely concluding the crystallization mechanism of ASW ultrathin films in relation to hydrophobicity and microscopic structure of substrates.

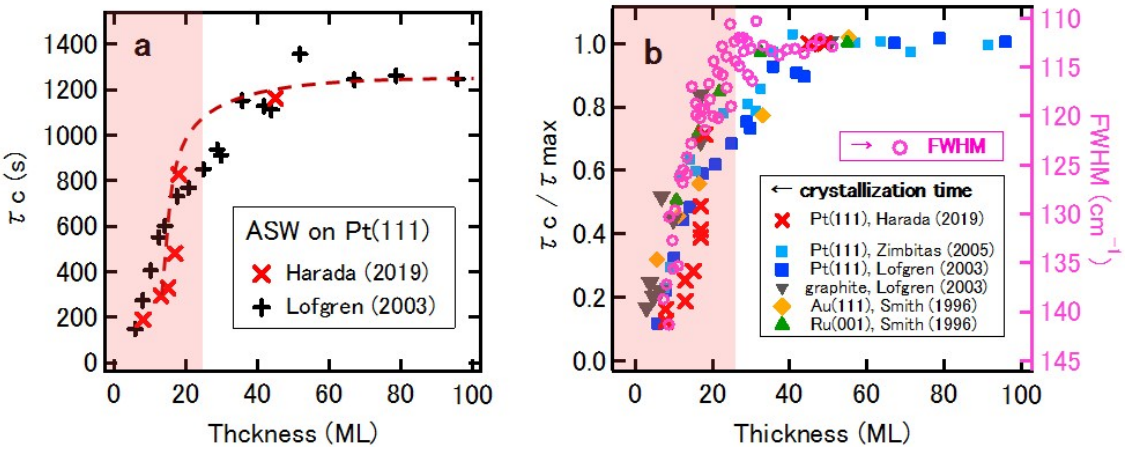

Figure S5. (a) Thickness dependence of crystallization time τ_c derived from the isothermal crystallization process of ASW films on Pt(111) annealed at 145 K. Red and black crosses indicate results of this work and those of previous work[8,9] by ITD, respectively. (b) Thickness dependence of τ_c normalized to τ_{c-max} of ASW films grown on various substrates, Pt(111),[8-10] graphite,[8,9] Au(111),[11] and Ru(001).[11] In previous reports,[8-11] τ_c was determined by ITD while our τ_c in this figure was obtained by isothermal IRAS measurements at 143 and 145 K. Full width of half maximum of the IRAS spectra of isotope diluted HDO (Fig. 4c) is also shown for comparison (Pink open circle).

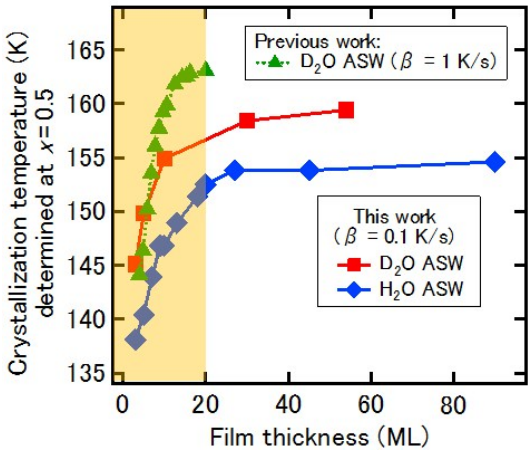

Figure S6. Thickness dependence of the crystallization temperature defined at "x=0.5" derived from TPD profiles of H_2O and D_2O ASW films on Pt(111). IRAS measurements in this work were conducted at heating rate of β = 0.1 K/s while TPD measurements in the previous work[18] were conducted at heating rate of β = 1 K/s. The difference of β (0.1 and 1 K/s) induces a difference of crystallization temperature of about 5 K. Note that crystallization temperature determined at x=0.5 instead of x=0.1 is plotted here for direct comparison with the results of ref.18.

4. Vibrational signature of H_2O superstructure on Pt(111)

Previous LEED,[10,.19,20] HAS,[21] and STM[22-24] observations reported $(\sqrt{37} \times \sqrt{37})R25.3°$ or $(\sqrt{39} \times \sqrt{39})R16.1°$ superstructures on Pt(111) at deposition temperatures around 130 K. In the superstructures, water molecules have shorter hydrogen-bond distances than that of bulk ice.[22,23] Feibelman et al.[25,26] attributed the peak at 1965 cm^{-1} of 1 ML H_2O films on Pt(111) to the OH stretching band of H_2O molecules with shorter hydrogen-bond distances (2.5-2.6 Å). We have also confirmed the peak at 1965 cm^{-1} in the IRAS spectra of ~1 ML H_2O films grown at 110 K and 140 K (Figure S7).

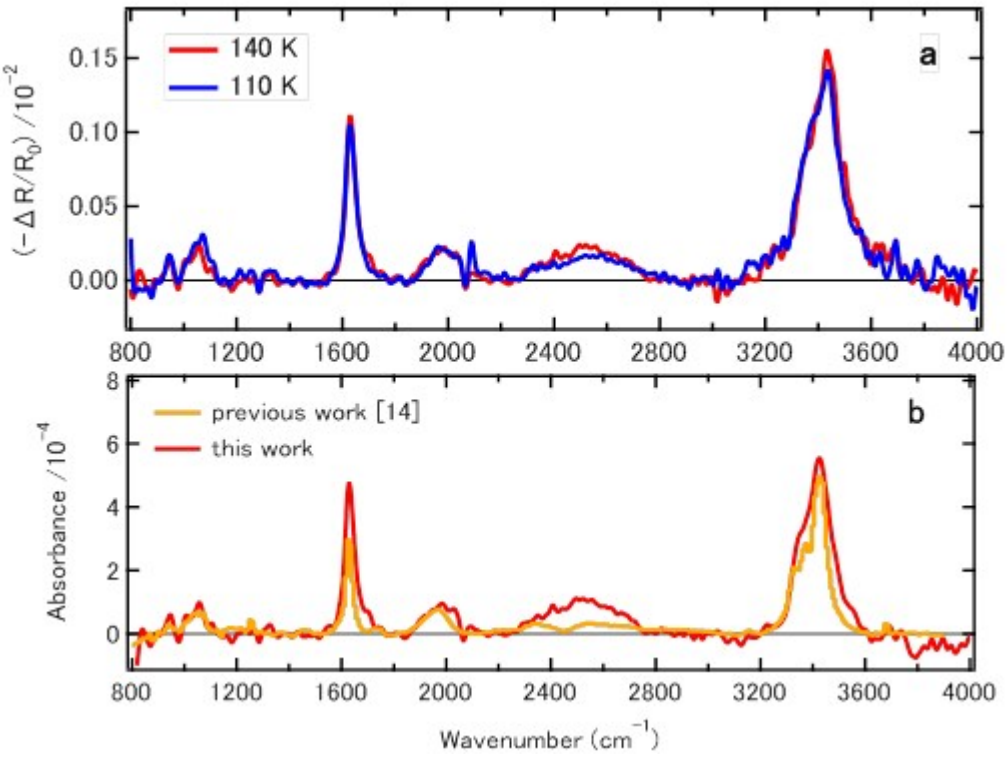

Figure S7. IRAS spectra of ~1 ML H_2O films on Pt(111). (a) Deposition temperature dependence. (b) Comparison with previous work.[25]

5. Activation energy of crystallization and Avrami index as a function of film thickness

The fittings of the crystallization curve with the Avrami equation (Figure 3a) give n and k as a function of thickness (Figures 3b and 3c). Figure S8a shows the Arrhenius plots of k. From these plots, we estimated the apparent activation energy of crystallization, E_A (Figures 3d and S8b).

As discussed in the main text, E_A is given by the sum of the activation energy for nucleation E_N and crystalline growth E_G as eq 4. The n dependence of E_A is also calculated with E_N = 140 kJ/mol and E_G = 40 kJ/mol reported previously for thick bulk ASW film.[1] Good agreement is observed for E_A at n~4 between our experimental result (~50 ML) and calculation with E_N = 140 kJ/mol and E_G = 40 kJ/mol. However, as shown in Figure S8b, calculated E_A for the constant E_N = 140 kJ/mol and E_G = 40 kJ/mol monotonically increases with decreasing n. This feature is in stark contrast to our experimental result, suggesting that E_N and E_G for the thermally relaxed ASW ultrathin films are not constant and decreases with decreasing the film thickness (n).

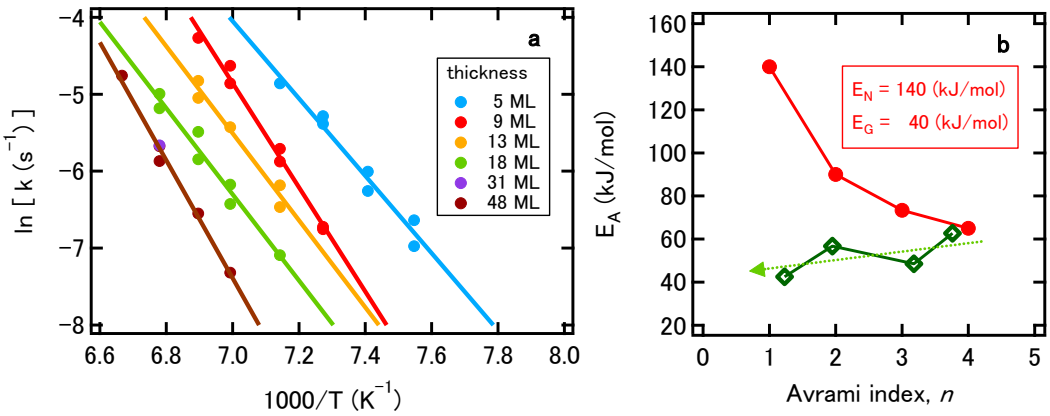

Figure S8. (a) Arrhenius plot of k derived from Avrami fitting (Figure 3a). (b) n dependence of E_A derived from the Arrhenius plot of k (open diamond) and that derived from eq 4 with constant E_N and E_G reported for the thick bulk ASW[1] (filled circle)

Supplementary references

(1) Kondo, T.; Kato, H. S.; Bonn, M.; Kawai, M. Deposition and Crystallization Studies of Thin Amorphous Solid Water Films on Ru(0001) and on CO-Precovered Ru(0001). *J. Chem. Phys.* **2007**, *127*, 094703.

(2) Backus, E. H. G.; Grecea, M. L.; Kleyn, A. W.; Bonn, M. Surface Crystallization of Amorphous Solid Water. *Phys. Rev. Lett.* **2004**, *92*, 236101.

(3) Yuan, C.; Smith, R. S.; Kay, B. D. Surface and Bulk Crystallization of Amorphous Solid Water Films: Confirmation of "Top-Down" Crystallization. *Surf. Sci.* **2016**, *652*, 350-354.

(4) Li, F; Skinner, J. L. Infrared and Raman Line Shapes for Ice Ih. I. Dilute HOD in H_2O and D_2O. *J. Chem. Phys.* **2010**, *132*, 204505.

(5) Shi, L.; Gruenbaum, S. M.; Skinner, J. L. Interpretation of IR and Raman Line Shapes for H_2O and D_2O Ice Ih. *J. Phys. Chem. B* **2012**, *116*, 13821-13830.

(6) Tainter, C. J.; Shi, L.; Skinner, J. L. Structure and OH-Stretch Spectroscopy of Low- and High-Density Amorphous Ices. *J. Chem. Phys.* **2014**, *140*, 134503.

(7) Kondo, T.; Kato, H. S., Kawai, M.; Bonn, M. The distinct vibrational signature of grain-boundary water innano-crystalline ice films. *Chem. Phys. Lett.* **2007**, 448, 121-126.

(8) Löfgren, P.; Ahlström, P.; Lausma, J.; Kasemo, B.; Chakarov, D. Crystallization Kinetics of Thin Amorphous Water Films on Surfaces. *Langmuir* **2003**, *19*, 265-274.

(9) Löfgren, P.; Ahlström, P.; Chakarov, D. V.; Lausmaa, J.; Kasemo, B. Substrate Dependent Sublimation Kinetics of Mesoscopic Ice Films. *Surf. Sci.* **1996**, *367*, L19-L25.

(10) Zimbitas, G.; Haq, S.; Hodgson, A. The Structure and Crystallization of Thin Water Films on Pt(111). *J. Chem. Phys.* **2005**, *123*, 174701.

(11) Smith, R. S.; Huang, C.; Wong, E. K. L.; Kay, B. D. Desorption and Crystallization Kinetics in Nanoscale Thin Films of Amorphous Water Ice. *Surf. Sci.* **1996**, *367*, L13-L18.

(12) Ahlström, P.; Löfgren, P.; Lausma, J.; Kasemo, B.; Chakarov, D. Crystallization Kinetics of Thin Amorphous Water Films on Surfaces: Theory and Computer Modeling. *Phys. Chem. Chem. Phys.* **2004**, 6, 1890-1898.

(13) Löfgren, P.; Ahlström, P.; Lausma, J.; Kasemo, B.; Chakarov, D. Crystallization Kinetics of Thin Amorphous Water Films on Surfaces. *Langmuir* **2003**, 19, 265-274.

(14) Löfgren, P.; Ahlström, P.; Chakarov, D. V.; Lausmaa, J.; Kasemo, B. Substrate Dependent Sublimation Kinetics of Mesoscopic Ice Films. *Surf. Sci.* **1996**, 367, L19-L25.

(15) Lupi, L.; Molinero, V. Does Hydrophilicity of Carbon Particles Improve Their Ice Nucleation Ability? *J. Phys. Chem. A* **2014**, 118, 7330-7337.

(16) Bi, Y.; Cabriolu, R.; Li, T. Heterogeneous Ice Nucleation Controlled by the Coupling of Surface Crystallinity and Surface Hydrophilicity. *J. Phys. Chem. C* **2016**, 120, 1507-1514.

(17) Zhang, Y.; Anim-Danso, E.; Bekele, S.; Dhinojwala, A. Effect of Surface Energy on Freezing Temperature of Water. *ACS Appl. Mater. Interfaces* **2016**, 8, 17583-17590.

(18) Kimmel, G. A.; Petrik, N. G.; Dohnálek, Z.; Kay, B. D. Crystalline Ice Growth on Pt(111) and Pd(111): Nonwetting Growth on a Hydrophobic Water Monolayer. *J. Chem. Phys.* **2007**, *126*, 114702.

(19) Haq, S. Harnett, J.; Hodgson, A. Growth of Thin Crystalline Ice Films on Pt(111). *Surf. Sci.* **2002**, *505*, 171-182.

(20) Harnett, J.; Haq, S.; Hodgson, A. Electron Induced Restructuring of Crystalline Ice Adsorbed on Pt(111). *Surf. Sci.* **2003**, *528*, 15-19.

(21) Glebov, A.; Graham, A. P.; Menzel, A.; Toennies, J. P. Orientational Ordering of Two-Dimensional Ice on Pt(111). *J. Chem. Phys.* **1997**, *106*, 9382-9385.

(22) Nie, S.; Feibelman, P. J.; Bartelt, N. C.; Thürmer, K. Pentagons and Heptagons in the First Water Layer on Pt(111). *Phys. Rev. Lett.* **2010**, *105*, 026102.

(23) Feibelman, P. J.; Bartelt, N. C.; Nie, S.; Thürmer, K. Interpretation of High-Resolution Images of the Best-Bound Wetting Layers on Pt(111). *J. Chem. Phys.* **2010**, *133*, 154703.

(24) Standop, S.; Redinger, A.; Morgenstern, Markus; Michely, T.; Busse, C. Molecular Structure of the H_2O Wetting Layer on Pt(111). *Phys. Rev. B* **2010**, *82*, 161412.

(25) Feibelman, P. J.; Kimmel, G. A.; Smith, R. S.; Petrik, N. G.; Zubkov, T.; Kay, B. D. A Unique Vibrational Signature of Rotated Water Monolayers on Pt(111): Predicted and Observed. *J. Chem. Phys.* **2011**, *134*, 204702.

(26) Kimmel, G. A.; Zubkov, T.; Smith, R. S.; Petrik, N. G.; Kay, B. D. Turning Things Downside Up: Adsorbate Induced Water Flipping on Pt(111). *J. Chem. Phys.* **2014**, *141*, 18C515.